Free-Surface Profiles, Velocity and Pressure Distributions on a Broad-Crested Weir: A Physical Study

Stefan Felder[1] and Hubert Chanson[2]

Abstract: Basic experiments were conducted on a large-size broad-crested weir with a rounded corner. Detailed free-surface, velocity, and pressure measurements were performed for a range of flow conditions. The results showed the rapid flow distribution at the upstream end of the weir and next to the weir brink at large flow rates. The flow properties above the crest were analyzed taking into account the nonuniform velocity and nonhydrostatic pressure distributions. Introducing some velocity and pressure correction coefficients, it is shown that critical flow conditions were achieved above the weir crest for $0.1 < x/L_{crest} < 1$. The velocity measurements highlighted a developing boundary layer. The data differed from the smooth turbulent boundary layer theory, although the present results were consistent with earlier studies. On average, the boundary stress was approximately $\tau_o/(\rho \times g \times H_1)$ 0.0015–0.0025. **DOI: 10.1061/(ASCE)IR.1943-4774.0000515.**

CE Database subject headings: Weirs; Velocity; Boundary layers; Pressure distribution; Irrigation.

Keywords: Broad-crested weir; Free-surface profile; Velocity distributions; Pressure distributions; Critical flow conditions; Turbulent boundary layer.

Introduction

A broad-crested weir is a flat-crested structure with a length, L_{crest}, larger than the flow thickness (Harrison 1967; Montes 1969) (Fig. 1). The crest is considered broad when the flow streamlines are parallel to the crest and the pressure distribution is hydrostatic (Bos 1976; Montes 1998). The discharge above the weir may be estimated as

$$Q = C_D \sqrt{g\left(\frac{2}{3}H_1\right)^3} B \quad (1)$$

where Q = flow rate; B = channel breadth; g = gravity acceleration; H_1 = upstream total head above the crest (Fig. 1); and C_D = dimensionless discharge coefficient (Henderson 1966; Chanson 2004).

The hydraulic characteristics of broad-crested weirs were studied during the nineteenth and twentieth centuries. Bélanger (1841, 1849) analyzed theoretically the overflow and derived Eq. (1) for the ideal case ($C_D = 1$). Successful physical studies included Bazin (1896), Woodburn (1932), Tison (1950), and Serre (1953). Hall (1962) and Isaacs (1981) studied the effects of developing a boundary layer on the overflow. Ramamurthy et al. (1988) investigated systematically the discharge characteristics of round-edged and square-edged weirs, and Sargison and Percy (2009) showed the influence of the weir inflow design on the bottom pressure distributions and discharge coefficient. Gonzalez and Chanson (2007) studying the flow above a large weir highlighted the effect of large vortical structures observed immediately upstream of the weir.

The purpose of this contribution is to document the free-surface profiles and pressure and velocity distributions on a horizontal broad-crested weir with a rounded nose. New experiments were performed in a large-sized facility. The results provide new insights into the vertical profiles of pressure and velocity on the broad-crest, including the boundary layer development and salient flow patterns.

Experimental Apparatus

New experiments were conducted at the University of Queensland in a test section 7 m long and 0.52 m wide. Waters were supplied from a large 1.5-m-deep feeding basin with a surface area of 2.9 × 2.2 m leading to a sidewall convergent (1.01 m long), with a 4.23:1 contraction ratio enabling a smooth and waveless inflow. The weir consisted of a 1-m-high, 0.52-m-wide, and 1.01-m-long flat horizontal crest with an upstream rounded corner (0.080 m radius). The crest was made of smooth, painted marine ply. Additional measurements were carried out in a 0.25-m-wide glass channel (Table 1).

A pump controlled with an adjustable frequency AC motor drive delivered the flow rate, enabling an accurate discharge adjustment in a closed-circuit system. Clear-water flow depths were measured on the channel centerline with a point gauge and by using photographs through the sidewalls. Sidewall photography was undertaken with digital Single Lens Reflex (dSLR) cameras, Canon EOS 450D and Pentax K-7, and the lens distortion correction was performed with the software PTLens version 8.7.8. The point gauge and photographic data yielded the same results within 0.5 mm. Pressure and velocity measurements were performed by using a Prandtl-Pitot tube (Ø = 3.0 mm). The tube was connected to an inclined manometer that gave both total and piezometric heads. The translation of the Pitot-Prandtl probe in the vertical direction was controlled by a fine adjustment traveling mechanism. The error on

[1]Ph.D. Student, School of Civil Engineering, The Univ. of Queensland, Brisbane QLD 4072, Australia.

[2]Professor in Hydraulic Engineering, School of Civil Engineering, The Univ. of Queensland, Brisbane QLD 4072, Australia (corresponding author). E-mail: h.chanson@uq.edu.au

Note. This manuscript was submitted on August 11, 2011; approved on June 1, 2012; published online on July 27, 2012. Discussion period open until May 1, 2013; separate discussions must be submitted for individual papers. This paper is part of the ***Journal of Irrigation and Drainage Engineering***, Vol. 138, No. 12, December 1, 2012. © ASCE, ISSN 0733-9437/2012/12-1068-1074/$25.00.

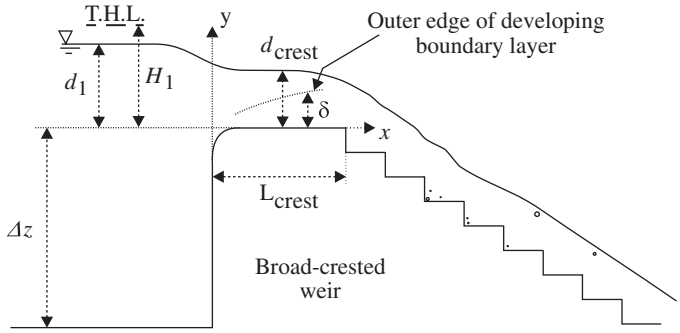

Fig. 1. Definition sketch of a broad-crested weir

the vertical position of the probe was less than 0.25 mm. The accuracy on the longitudinal position was estimated as $\Delta x < +/- 1$ mm. The accuracy on the transverse position of the probe was less than 1 mm.

Basic Flow Patterns

The inflow conditions were quiescent for all investigated flow conditions. The free-surface upstream of and above the crest was very smooth. Immediately upstream of the weir crest, the flow accelerated, was critical above the crest, and became supercritical on the downstream steep slope (Fig. 1). Next to the upstream end of the crest, the flow was rapidly varied and characterized by some free-surface curvature (Fig. 2) and some rapid change in pressure and velocity distributions. Fig. 2 presents some typical free-surface profiles recorded above the crest. The data highlighted that the free-surface profile above the weir crest is not horizontal, as was previously reported (Woodburn 1932; Harrison 1967). For some flow conditions, some wavy profile was observed above the crest; for example, for $H_1/L_{crest} = 0.06$ and 0.10 in Fig. 2. These might be linked with the interactions of the developing boundary layer with the main flow, as discussed by Isaacs (1981).

Above the broad crest, the specific energy was minimal, and critical flow conditions took place. Although the water surface was not horizontal, the depth-averaged specific energy was basically constant above the entire crest. The depth-averaged specific energy above the crest is commonly expressed following Liggett (1993) and Chanson (2006) as

$$H = \frac{\int_0^d \left(\frac{v_x^2}{2 \times g} + z + \frac{P}{\rho \times g}\right) \times dy}{d} = \beta \times \frac{V^2}{2 \times g} + \Lambda \times d \quad (2)$$

where H = depth-averaged specific energy; d = flow depth; P = pressure; V = depth-averaged velocity; y = vertical elevation above the crest; β = momentum correction coefficient or Boussinesq coefficient; and Λ = pressure correction coefficient defined as

$$\Lambda = \frac{1}{2} + \frac{1}{d} \times \int_0^d \frac{P}{\rho \times g \times d} \times dy \quad (3)$$

Table 1. Experimental Investigations of Horizontal Broad-Crested Weirs

Experiment	L_{crest} (m)	Δz (m)	B (m)	Q (m^3/s)	H_1 (m)	H_1/L_{crest}	Remarks
Sharp-edged weir							
Bazin (1896)	0.40	0.75	2.0	—	0.064–0.402	0.159–1.0	Sér. 113
	0.80	0.75	2.0	—	0.062–0.42	0.0779–0.527	Sér. 114
	1.99	0.75	2.0	—	0.06–0.447	0.03–0.225	Sér. 115
Woodburn (1932)	3.05	0.533	0.6096	—	0.1524–0.457	0.05–0.2	
Tison (1950)	1.80	0.30	0.50	0.0073–0.041	0.042–0.132	0.023–0.073	
Rao and Muralidhar (1963)	0.10–3.0	0.3	0.610	up to 0.14	0.03–0.25	0.017–1.9	
Mos (1972)	0.15	0.152	0.610	—	0.051 and 0.76	0.336 and 0.5	
	0.381	0.152	0.610	—	0.038	0.10	
	0.762	0.152	0.610	—	0.033 and 0.048	0.043 and 0.063	
Sargison and Percy (2009)	0.5	0.25	0.20	0.004–0.015	0.06–0.14	0.12–0.28	Vertical wall
				0.005–0.016	0.06–0.14	0.13–0.28	1H:1V upstream wall
				0.005–0.018	0.07–0.13	0.13–0.3	2H:1V upstream wall
Rounded-edged weir							
Bazin (1896)	0.90	0.75	2.0	—	0.054–0.402	0.06–0.446	$R = 0.10$ m, Sér. 116
	2.09	0.75	2.0	—	0.048–0.407	0.023–0.195	$R = 0.10$ m, Sér. 117
Woodburn (1932)	3.05	0.533	0.6096		0.1524–0.457	0.05–0.2	$R = 0.051$–0.203 m
Vierhout (1973)	0.40	0.25	0.50	0.025–0.070	—	0.24–0.48	$R = 0.10$ m
	1.20	0.25	0.50	0.065–0.100	—	0.155–0.202	$R = 0.10$ m
Isaacs (1981)	0.42	0.0646	0.25	0.001–0.07	0.015–0.0675	0.036–0.161	
Gonzalez and Chanson (2007)							
Geometry 1	0.60	0.90	1.0	0.046–0.182	0.09–0.225	0.15–0.375	$R = 0.057$ m, vertical upstream wall
Geometry 2	0.88	0.90	1.0	0.05–0.26	0.096–0.29	0.10–0.32	$R = 0.057$ m, vertical upstream wall
Geometry 3	0.617	0.99	1.0	0.0064–0.17	0.023–0.21	0.037–0.337	$R = 0.057$ m, 0.25 m overhanging crest
Geometry 4	0.617	0.99	1.0	0.0064–0.21	0.023–0.24	0.037–0.39	$R = 0.057$ m, vertical upstream wall
Small weir	0.42	0.0646	0.25	0.001–0.005	0.015–0.075	0.036–0.18	Vertical upstream wall
Present study							
Large weir	1.01	1.0	0.52	0.0025–0.142	0.021–0.30	0.021–0.297	$R = 0.080$ m, vertical upstream wall
Small weir	0.42	0.0646	0.25	0.0012–0.0154	0.019–0.111	0.047–0.265	Vertical upstream wall

Note: H_1 upstream head above crest elevation; Q = water flow rate; R = radius of curvature; — = not available.

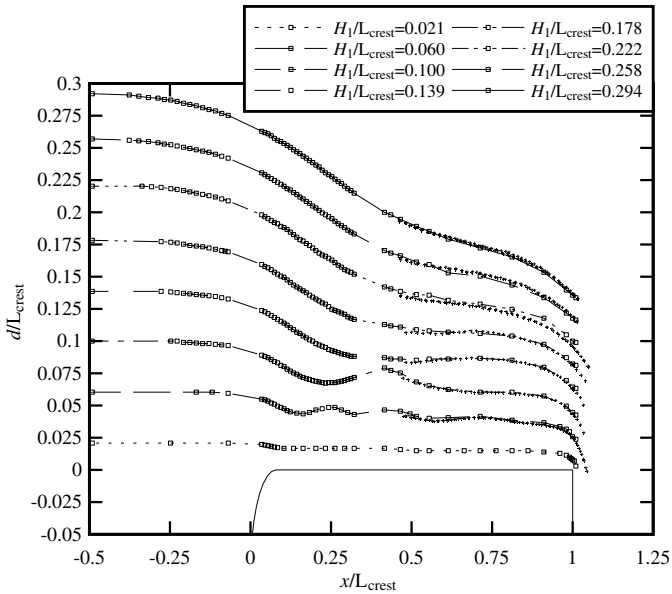

Fig. 2. Dimensionless free-surface profiles above a broad-crested weir; both point gauge (small squares and dashed line) and photographic (small crosses) data are presented; weir profile is shown in black (note distorted scale)

For a uniform flow above a flat broad crest with the streamlines parallel to the crest, the velocity distribution is uniform ($\beta = 1$), the pressure is hydrostatic ($\Lambda = 1$), and Eq. (2) equals the classical result

$$H = \frac{V^2}{2 \times g} + d = \frac{3}{2} \times \sqrt[3]{\frac{Q^2}{g \times B^2}} \tag{4}$$

In practice, however, the velocity distributions were not uniform along the crest because of the bed friction above the crest, and a turbulent boundary layer developed. Furthermore, the streamlines and free-surface were not parallel to the crest everywhere (Fig. 2).

When the specific energy is at a minimum, the flow depth above the crest is critical (Bakhmeteff 1932; Henderson 1966) and must satisfy one of the following four physical solutions (Chanson 2006):

$$\frac{d}{H} \times \Lambda = \sqrt[3]{\frac{1 - 2 \times \beta \times {C_D}^2 \times \Lambda^2}{27} + \Lambda^3 \times \sqrt{\Delta}} + \sqrt[3]{\frac{1 - 2 \times \beta \times {C_D}^2 \times \Lambda^2}{27} - \Lambda^3 \times \sqrt{\Delta}} + \frac{1}{3} \qquad \Delta > 0 \tag{5a}$$

$$\frac{d}{H} \times \Lambda = \frac{2}{3} \qquad \Delta = 0 \tag{5b}$$

$$\frac{d}{H} \times \Lambda = \frac{2}{3} \times \left(\frac{1}{2} + \cos\frac{\varepsilon}{3}\right) \qquad \Delta < 0 \text{ \& Solution } S1 \tag{5c}$$

$$\frac{d}{H} \times \Lambda = \frac{2}{3} \times \frac{1 - \cos\frac{\varepsilon}{3} + \sqrt{3 \times [1 - (\cos\frac{\varepsilon}{3})^2]}}{2} \qquad \Delta < 0 \text{ \& Solution } S3 \tag{5d}$$

where

$$\cos\varepsilon = 1 - 2 \times \beta \times {C_D}^2 \times \Lambda^2 \tag{6}$$

and the discriminant Δ equals

$$\Delta = \frac{4 \times \beta \times {C_D}^2 \times \Lambda^2}{(3 \times \Lambda)^6} \times (\beta \times {C_D}^2 \times \Lambda^2 - 1) \tag{7}$$

Eq. (5) expresses the flow depth at critical flow conditions in the general case when $\beta > 1$ and $\Lambda \neq 1$. Present experimental data were tested against Eq. (5). Typical results are presented in Fig. 3 in terms of the dimensionless water depth $d \times \Lambda / H_1$ as a function of $\beta \times {C_D}^2 \times \Lambda^2$, where β, C_D, and Λ were calculated based on the pressure and velocity distribution data. The whole data set is also reported in the appendix. The C_D was estimated using Eq. (1), in which the discharge per unit width was deduced from the equation of conservation of mass

$$\frac{Q}{B} = \int_0^d v_x \times dy \tag{8}$$

In Fig. 3, each data set regroups the flow depth measurements for $0.1 < x/L_{crest} < 1$, and they are compared with experimental results obtained above circular crested weirs (Fawer 1937; Vo 1992) and in undular flows (Chanson 2005). The present results showed an overall reasonable agreement between data and theory; in particular, the solutions S1 and S3 ($\Delta < 0$) along the entire weir crest (Fig. 3). The agreement between Eq. (5) and the data highlighted that the assumption of critical flow conditions holds along the crest ($0.1 < x/L_{crest} < 1$) despite the boundary layer development and the nonhorizontal free-surface.

The flow depth above the crest differed from the classical expression $\sqrt[3]{Q^2/(g \times B^2)}$ because of the nonuniform velocity and nonhydrostatic pressure distributions.

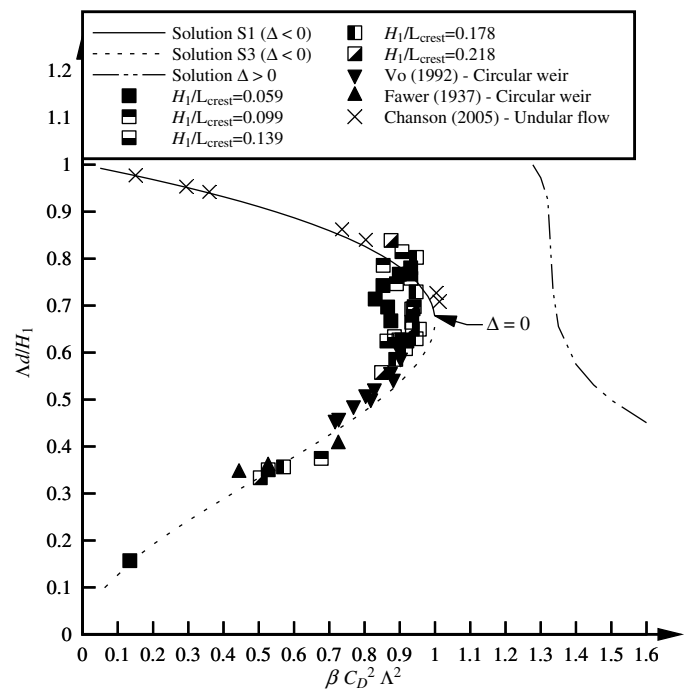

Fig. 3. Dimensionless flow depth above the weir crest $d \times \Lambda / H_1$ as a function of $\beta \times {C_D}^2 \times \Lambda^2$; comparison between broad-crested weir data (present study, $0.1 < x/L_{crest} < 1$), analytical solutions [Eq. (5)], circular crested weir data (Fawer 1937; Vo 1992), and undular flow data (Chanson 2005)

Velocity and Pressure Distributions

The vertical distributions of velocity and pressure were measured along the crest for a range of flow conditions ($0.02 < H_1/L_{crest} < 0.3$). The experimental data showed systematically the redistributions of pressure and velocity profiles at the upstream and downstream ends of the broad crest (Fig. 4). For $x/L_{crest} < 0.2$, the pressure gradient was typically less hydrostatic, and the velocity profile had a shape close to that predicted by the ideal-fluid flow theory and flow net considerations. At the downstream end, the free-surface curvature became pronounced as the flow accelerated near the brink (Fig. 2). At the brink, the velocity and pressure profiles were similar to those observed at a free overfall (Henderson 1966) (Fig. 4). Some typical velocity and pressure distribution data are shown in Fig. 4, and the figure captions detail the flow conditions. Figs. 4(a and b) present some dimensionless velocity profiles for two dimensionless heads above the crest. The velocity data at $x/L_{crest} = -0.065$ upstream of the crest were the longitudinal velocity component data only. Fig. 4(c) shows the dimensionless pressure distributions for the experiment presented in Fig. 4(b); the solid line (slope 1:1) is the hydrostatic pressure distribution. In Fig. 4(c), the pressure distributions at $x/L_{crest} = 0.11$ and 0.78 differ from the hydrostatic profile and are compared with an inviscid solution of the Boussinesq equation (Montes and Chanson 1998) that was calculated based on the measured free-surface slope and curvature. Although the effect of boundary friction could be included (Castro-Orguaz and Chanson 2011), it is believed that the observed nonhydrostatic pressure distribution resulted primarily from an inviscid velocity redistribution rather than from boundary friction effects.

The rapid flow redistribution at the upstream end of the weir crest was associated with the development of a turbulent boundary layer. At the upstream end of the crest, the flow was essentially irrotational, but the no-slip condition at the crest invert ($y = 0$) induced a boundary layer growth. The boundary layer development was estimated from the measured velocity profiles. Results are presented in Fig. 5, in which they are compared with the boundary layer growth above a smooth flat plate in the absence of pressure gradient for two flow conditions. For the present data, the boundary layer thickness development was best correlated by

$$\frac{\delta}{x} \sim \left(\frac{x}{k_s}\right)^{-0.124} \qquad x/L_{crest} < 0.7 \tag{9}$$

where δ = boundary layer thickness defined in terms of 99% of the free-stream velocity; and k_s = equivalent sand roughness height ($k_s = 0.5$ mm). The boundary layer growth was approximately $\delta \sim x^{0.87}$ compared to a smooth turbulent boundary layer growth of $\delta \sim x^{0.8}$ (Schlichting 1979; Chanson 2009). The free-surface data implied a slightly favorable longitudinal pressure gradient, and it is

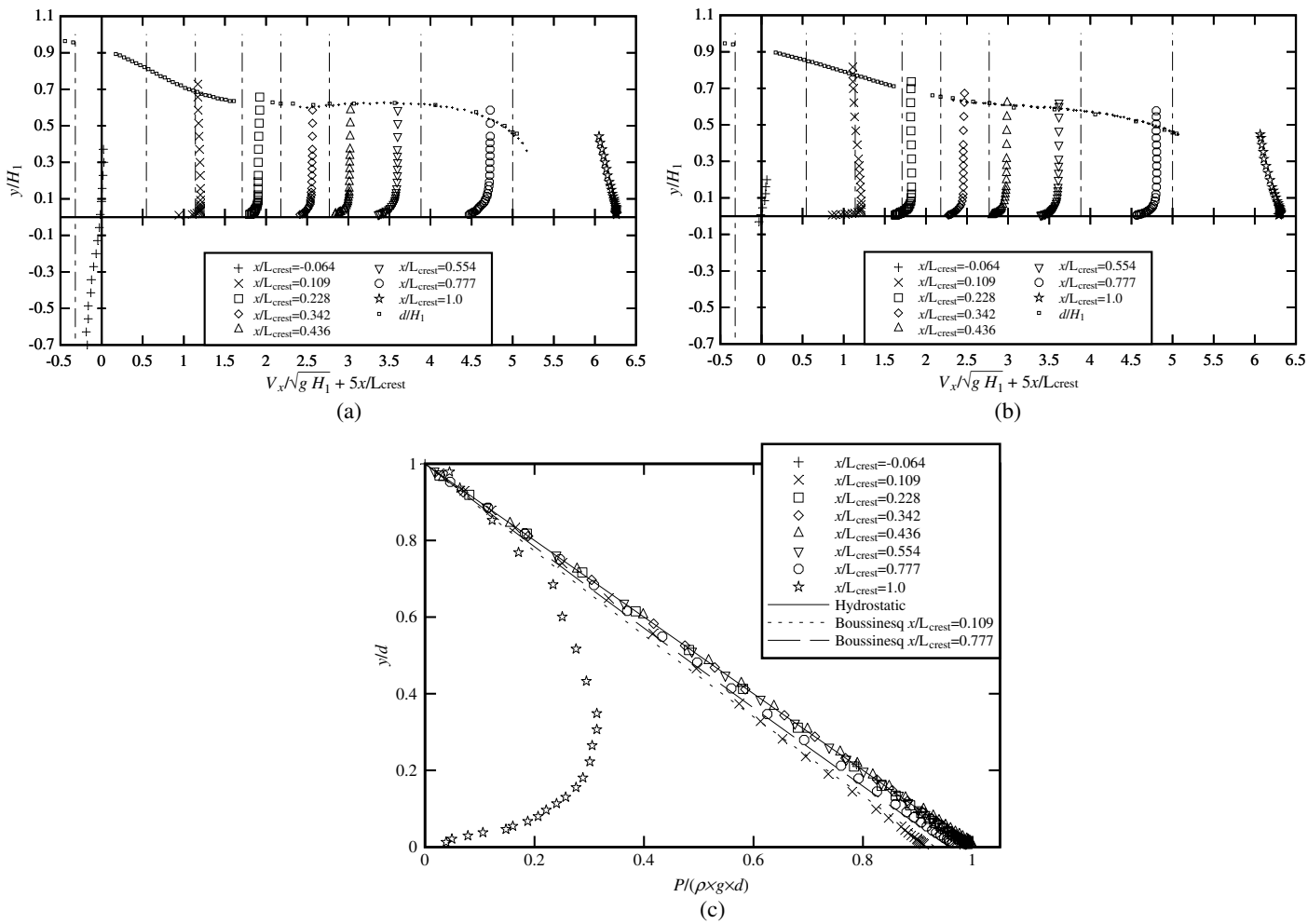

Fig. 4. Dimensionless distributions of velocity and pressure along the broad-crested weir: (a) velocity distributions for $H_1/L_{crest} = 0.139$; (b) velocity distributions for $H_1/L_{crest} = 0.224$; (c) pressure distributions for $H_1/L_{crest} = 0.224$; comparison with the hydrostatic pressure and a Boussinesq equation solution for $x/L_{crest} = 0.109$ and 0.777

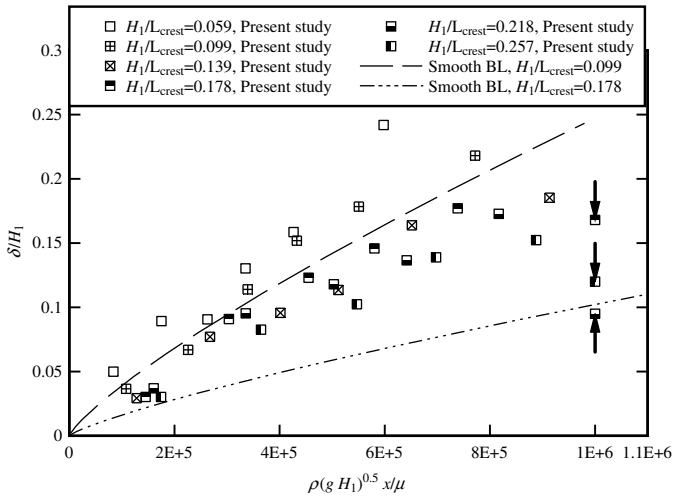

Fig. 5. Dimensionless boundary layer thickness δ/H_1; comparison with the smooth boundary layer theory for $H_1/L_{crest} = 0.099$ and 0.178

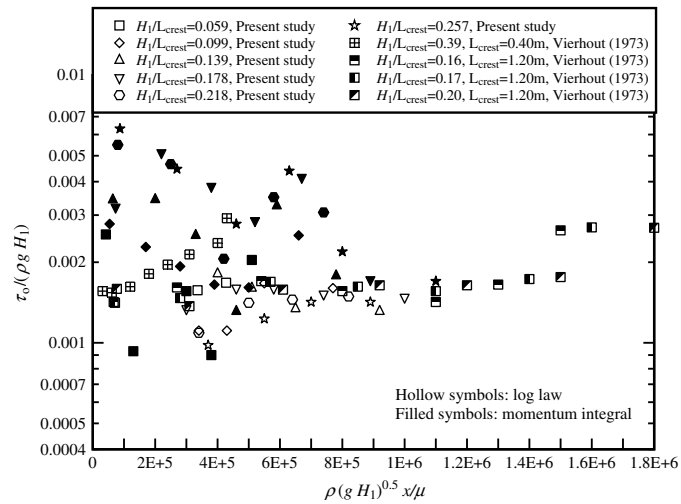

Fig. 6. Dimensionless boundary shear stress $\tau_o/(\rho \times g \times H_1)$ above the crest; comparison between logarithmic law and momentum integral equation results and the data of Vierhout (1973) obtained with a Preston tube

acknowledged that the comparison with the zero pressure gradient boundary layer theory might have some limitation.

The boundary layer data further showed an apparent reduction in boundary layer thickness at the downstream end of the crest for the larger discharges, i.e., $H_1/L_{crest} > 0.18$. This is highlighted in Fig. 5 (symbols with arrow on right). It is believed to be caused by some velocity redistributions induced by the free-surface and streamline curvature of the flow. A similar flow redistribution at the crest's downstream end was documented by Vierhout (1973) and Matos (personal communication, 2011).

Discussion

In a smooth turbulent boundary layer, the solution of Prandlt's mixing length yields the law of the wall characterizing the velocity profile in the inner flow region, as follows:

$$\frac{v_x}{V_*} = 2.5 \times Ln\left(\frac{\rho \times V_* \times y}{\mu}\right) + 5 \qquad y/\delta < 0.15 \qquad (10)$$

where V_* = shear velocity ($V_* = \sqrt{\tau_o/\rho}$); μ = dynamic viscosity; and τ_o = boundary shear stress (Schlichting 1979; Montes 1998). The boundary shear stress over the crest was estimated from the velocity measurements in the developing boundary layer by the best fit of the data, with Eq. (10) in the inner region. The results were compared with the boundary shear stress calculated from the von Karman momentum integral equation

$$\frac{\tau_o}{\rho} = \frac{\partial}{\partial x}(U^2 \times \delta_2) + U \times \delta_1 \times \frac{\partial U}{\partial x} \qquad (11)$$

where U = free-stream velocity: $U = v_x(y > \delta)$; and δ_1 and δ_2 are the displacement and momentum thicknesses (Liggett 1994; Chanson 2009), respectively. The boundary shear stress data are presented in Fig. 6; both results derived from Eqs. (10) and (11) are presented and compared with the data Vierhout (1973) obtained by using a Preston tube. Despite some scatter, the data yielded a dimensionless boundary shear stress of $\tau_o/(\rho \times g \times H_1) = 0.0015$ and 0.0025 on average using Eqs. (10) and (11), respectively, whereas the data of Vierhout (1973) gave $\tau_o/(\rho \times g \times H_1) = 0.0016$ on average.

The discharge per unit width was calculated from the integration of the measured velocity profiles [Eq. (8)] on the middle of the crest ($x/L_{crest} = 0.55$). The data are summarized in Fig. 7 in terms of the dimensionless discharge coefficient C_D [Eq. (1)], and they are compared with previous studies of broad-crested weirs obtained with an upstream rounded edge (Bazin 1896; Vierhout 1973; Gonzalez and Chanson 2007), square edge (Bazin 1896; Sargison and Percy 2009), and inclined upstream wall (Sargison and Percy 2009) (Table 1). Fig. 7 illustrates the lower discharge capacity of square-edged weirs linked with the adverse role of the upstream separation bubble (Mos 1972).

The present results showed a slight increase in the discharge coefficient with an increasing head above the crest, similar to previous studies. For large dimensionless heads above the crest, the weir would no longer act as a broad-crest, and the discharge

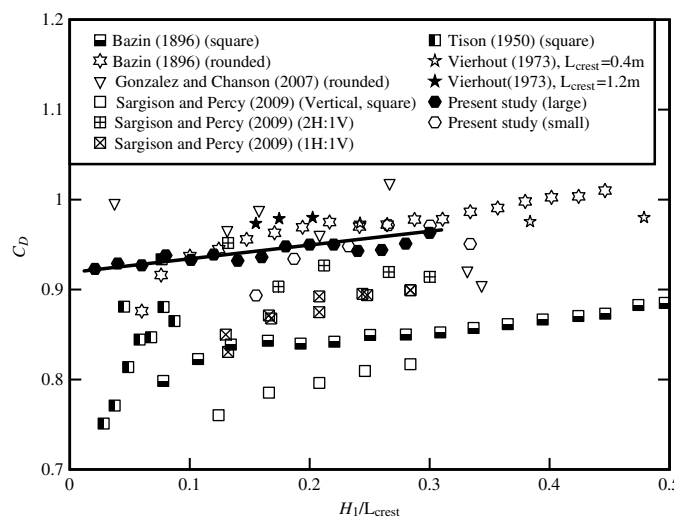

Fig. 7. Dimensionless discharge coefficients for broad-crested weirs; comparison with Eq. (12) and previous studies with square-edge (Bazin 1896; Sargison and Percy 2009), rounded edge (Bazin 1896; Vierhout 1973; Gonzalez and Chanson 2007), and inclined upstream wall (Sargison and Percy 2009)

coefficient would tend to values close to those observed on rounded weirs (e.g., circular or ogee). Overall, the dimensionless discharge coefficient data was best correlated by

$$C_D = 0.92 + 0.153 \times \frac{H_1}{L_{crest}} \quad \text{Large weir } (\Delta z = 1.0 \text{ m}) \quad (12)$$

for $0.02 < H_1/L_{crest} < 0.3$. Eq. (12) is shown in Fig. 7.

The present data trend differed from the data of Gonzalez and Chanson (2007), who observed the occurrence of irregular corner eddies next to the sidewalls immediately upstream of the vertical upstream wall, associated with instabilities affecting the overflow motion. In the present study, the inflow conditions were very smooth, and no irregular vortice generation was observed.

Conclusion

Some basic experiments were conducted on a large broad-crested weir with rounded corners. Both free-surface profiles and pressure and velocity distributions were recorded for a relatively wide range of flow conditions ($0.02 < H_1/L_{crest} < 0.3$).

The results highlighted the rapid redistributions of velocity and pressure fields at the upstream and downstream ends of the crest, although the flow was critical along the crest (Fig. 3). This was rarely documented in a large facility under controlled flow conditions. At the upstream end, the flow motion was irrotational, and the pressure and velocity distributions were affected by the streamline and free-surface curvature. At the downstream end of the crest, the flow properties were close to those observed at the brink of an overfall. The velocity distributions measurements highlighted a developing boundary layer. Although the data differed from the smooth turbulent boundary layer theory, the results were consistent with earlier studies. The dimensionless boundary stress was on average $\tau_o/(\rho \times g \times H_1) \sim 0.0015$–$0.0025$, and the result was nearly independent of the measurement technique; namely, using the best fit to the log-law and the momentum integral equation. A correlation was derived for the dimensionless discharge coefficient C_D that was close to earlier results with rounded broad crests, and C_D was typically larger than for square broad crests (Fig. 7).

Appendix. Experimental Investigations of Pressure and Velocity Distributions in Critical Flow Conditions

Ref. (mm)	H_1 (m)	H_1/L_{crest}	x/L_{crest}	C_D	β	Λ	$\beta \times C_D^2 \times \Lambda^2$	$\Lambda \times d/H_1$
60	0.06	0.059	0.11	1.000	0.959	0.986	0.931	0.780
60	0.06	0.059	0.23	0.993	1.012	0.949	0.899	0.767
60	0.06	0.059	0.34	0.968	1.012	0.948	0.852	0.743
60	0.06	0.059	0.44	0.971	1.015	0.931	0.830	0.714
60	0.06	0.059	0.55	0.927	1.015	0.996	0.865	0.697
60	0.06	0.059	0.78	0.925	1.020	1.001	0.875	0.668
60	0.06	0.059	1.00	0.997	1.029	0.362	0.134	0.157
100	0.1	0.099	0.11	0.920	1.006	1.001	0.853	0.786
100	0.1	0.099	0.23	0.948	1.009	1.019	0.941	0.698
100	0.1	0.099	0.34	0.974	1.012	0.985	0.931	0.758
100	0.1	0.099	0.44	0.961	1.026	0.969	0.890	0.746
100	0.1	0.099	0.55	0.962	0.995	1.007	0.934	0.665
100	0.1	0.099	0.78	0.950	1.014	0.995	0.906	0.627
100	0.1	0.099	1.00	0.983	1.011	0.832	0.677	0.375
140	0.14	0.139	0.11	0.947	1.008	1.001	0.906	0.815
140	0.14	0.139	0.23	0.954	1.007	1.011	0.938	0.693
140	0.14	0.139	0.34	0.950	1.009	1.005	0.920	0.625
140	0.14	0.139	0.44	0.935	1.009	1.009	0.898	0.627
140	0.14	0.139	0.55	0.932	1.011	1.003	0.885	0.634
140	0.14	0.139	0.78	0.924	1.013	1.000	0.864	0.625
140	0.14	0.139	1.00	0.971	1.010	0.744	0.527	0.351
180	0.18	0.178	0.11	0.988	1.006	0.983	0.947	0.803
180	0.18	0.178	0.23	0.960	1.006	1.010	0.946	0.729
180	0.18	0.178	0.34	0.966	1.007	1.008	0.956	0.650
180	0.18	0.178	0.44	0.962	1.008	1.007	0.946	0.629
180	0.18	0.178	0.55	0.949	1.009	1.005	0.916	0.608
180	0.18	0.178	0.78	0.943	1.011	0.994	0.889	0.585
180	0.18	0.178	1.00	0.973	1.008	0.773	0.570	0.357
220	0.22	0.218	0.11	0.957	1.007	0.974	0.875	0.839
220	0.22	0.218	0.23	0.956	1.005	1.005	0.928	0.767
220	0.22	0.218	0.34	0.962	1.005	1.003	0.934	0.693
220	0.22	0.218	0.44	0.957	1.006	1.008	0.936	0.650
220	0.22	0.218	0.55	0.950	1.006	1.004	0.915	0.625
220	0.22	0.218	0.78	0.932	1.006	0.985	0.848	0.558
220	0.22	0.218	1.00	0.974	1.008	0.726	0.504	0.333
260	0.26	0.257	0.11	0.952	1.008	0.963	0.847	0.820
260	0.26	0.257	0.23	0.951	1.005	0.997	0.905	0.769
260	0.26	0.257	0.34	0.945	1.005	0.932	0.780	0.649
260	0.26	0.257	0.44	0.945	1.005	1.004	0.904	0.654
260	0.26	0.257	0.55	0.943	1.005	0.999	0.893	0.621
260	0.26	0.257	0.78	0.954	1.006	0.983	0.884	0.567
260	0.26	0.257	1.00	0.970	1.007	0.718	0.488	0.329

Acknowledgments

The authors thank Ahmed Ibrahim and Jason Van Der Gevel (The Univ. of Queensland) for the technical assistance. The financial support of the Australian Research Council (Grant DP0878922) is acknowledged. The first author was supported by a Univ. of Queensland research scholarship.

Notation

The following symbols are used in this paper:

B = channel breadth (m);
C_D = dimensionless discharge coefficient;
d = water depth (m);
g = gravity acceleration (m/s^2);
H = total head (m);
H_1 = upstream total head (m) measured above the crest;
k_s = equivalent sand roughness height (m);
L_{crest} = crest length (m) measured in the flow direction;
P = pressure;
Q = water discharge (m^3/s);
R = radius of curvature (m);
U = free-stream velocity (m/s);
V = flow velocity (m/s), $V = Q/(d \times B)$;
V_* = shear velocity (m/s);
v_x = longitudinal velocity component (m/s);
x = longitudinal distance (m) measured from the crest upstream end;
y = distance (m) normal to the crest invert;
β = momentum correction coefficient, also called Boussinesq coefficient;
Δ = discriminant;
Δz = weir height (m) above upstream channel invert;
δ = boundary layer thickness (m);
δ_1 = boundary layer displacement thickness (m);
δ_2 = boundary layer momentum thickness (m);

ε = dimensionless term;
Λ = pressure correction coefficient;
μ = dynamic viscosity of water (Pa.s);
ρ = water density (kg/m^3);
τ_o = boundary shear stress (Pa); and
Ø = diameter (m).

References

Bakhmeteff, B. A. (1932). *Hydraulics of open channels*, 1st Ed., McGraw-Hill, New York.

Bazin, H. (1896). "Expériences nouvelles sur l'ecoulement par déversoir [recent experiments on the flow of water over weirs]." *Mémoires et Documents, Annales des Ponts et Chaussées*, Paris, France, Sér. 7, Vol. 12, 2nd Sem., 645–731 Plates (in French).

Bélanger, J. B. (1841). "Notes sur l'hydraulique [notes on hydraulic engineering]." *Ecole Royale des Ponts et Chaussées*, Paris, France, Session 1841–1842 (in French).

Bélanger, J. B. (1849). "Notes sur le cours d'hydraulique [notes on the hydraulics subject]." *Mém. Ecole Nat. Ponts et Chaussées*, Paris, France (in French).

Bos, M. G. (1976). *Discharge measurement structures*, Publication No. 161, Delft Hydraulic Laboratory, Delft, Netherlands.

Castro-Orgaz, O., and Chanson, H. (2011). "Near-critical free-surface flows: real fluid flow analysis." *Environ. Fluid Mech.*, 11(5), 499–516.

Chanson, H. (2004). *The hydraulics of open channel flows: An introduction*, 2nd Ed., Butterworth-Heinemann, Oxford, United Kingdom.

Chanson, H. (2005). "Physical modelling of the flow field in an undular tidal bore." *J. Hydraul. Res.*, 43(3), 234–244.

Chanson, H. (2006). "Minimum specific energy and critical flow conditions in open channels." *J. Irrig. Drain. Eng.*, 132(5), 498–502.

Chanson, H. (2009). *Applied hydrodynamics: An introduction to ideal and real fluid flows*, CRC, Taylor & Francis Group, Leiden, Netherlands.

Fawer, C. (1937). "Etude de quelques ecoulements permanents à filets courbes [study of some steady flows with curved streamlines]." Ph.D. thesis, Imprimerie La Concorde, Lausanne, Switzerland (in French).

Gonzalez, C. A., and Chanson, H. (2007). "Experimental measurements of velocity and pressure distribution on a large broad-crested weir." *Flow Meas. Instrum.*, 18(3–4), 107–113.

Hall, G. W. (1962). "Analytical determination of the discharge characteristics of broad-crested weirs using boundary layer theory." *ICE Proc.*, 22, 177–190.

Harrison, A. J. M. (1967). "The streamlined broad-crested weir." *ICE Proc.*, 38, 657–678.

Henderson, F. M. (1966). *Open channel flow*, MacMillan, New York.

Isaacs, L. T. (1981). "Effects of laminar boundary layer on a model broad-crested weir." *Research Rep. No. CE28*, Dept. of Civil Engineering, Univ. of Queensland, Brisbane, Australia.

Liggett, J. A. (1993). "Critical depth, velocity profiles and averaging." *J. Irrig. Drain. Eng.*, 119(2), 416–422.

Liggett, J. A. (1994). *Fluid mechanics*, McGraw-Hill, New York.

Montes, J. S. (1969). "The streamlined broad-crested weir. Discussion." *ICE Proc.*, 42, 576–578.

Montes, J. S. (1998). *Hydraulics of open channel flow*, ASCE, New York.

Montes, J. S., and Chanson, H. (1998). "Characteristics of undular hydraulic jumps. Results and calculations." *J. Hydraul. Eng.*, 124(2), 192–205.

Mos, W. D. (1972). "Flow separation at the upstream edge of a square-edged broad-crested weir." *J. Fluid Mech.*, 52, 307–320.

Ramamurthy, A. S., Tim, U. S., and Rao, M. V. J. (1988). "Characteristics of square-edged and round-nosed broad-crested weirs." *J. Irrig. Drain. Eng.*, 114(1), 61–73.

Rao, N. S. Govinda, and Muralidhar, D. (1963). "Discharge characteristics of weirs of finite crest width." *J. La Houille Blanche*, 18(5), 537–545.

Sargison, J. E., and Percy, A. (2009). "Hydraulics of broad-crested weirs with varying side slopes." *J. Irrig. Drain. Eng.*, 135(1), 115–118.

Schlichting, H. (1979). *Boundary layer theory*, 7th Ed., McGraw-Hill, New York.

Serre, F. (1953). "Contribution à l'etude des ecoulements permanents et variables dans les canaux [Contribution to the study of permanent and non-permanent flows in channels]." *J. La Houille Blanche*, (6), 830–872 (in French).

Tison, L. J. (1950). "Le déversoir epais [broad-crested weir]." *J. La Houille Blanche*, (4), 426–439 (in French).

Vierhout, M. M. (1973). "On the boundary layer development in round broad-crested weirs with a rectangular control section." *Rep. No. 3*, Laboratory of Hydraulics and Catchment Hydrology, Agricultural Univ., Wageningen, Netherlands.

Vo, N. D. (1992). "Characteristics of curvilinear flow past circular-crested weirs." Ph.D. thesis, Concordia Univ., Montreal, PQ.

Woodburn, J. G. (1932). "Tests of broad-crested weirs." *Transactions*, 96, 387–416.